

1 **Fire fragility curves for industrial steel pipe-racks integrating demand** 2 **and capacity uncertainties**

3 *Luca Possidente*, Department of Civil, Environmental and Mechanical Engineering, University of
4 Trento, Via Mesiano 77, 38123 Trento, Italy and Department of Civil, Environmental & Geomatic
5 Engineering, University College London, London, United Kingdom

6 *Jerome Randaxhe*, ICB, Ingenieurs Conseils en Batiments, Rodange, Luxembourg

7 *Nicola Tondini*, Department of Civil, Environmental and Mechanical Engineering, University of
8 Trento, Via Mesiano 77, 38123 Trento, Italy

9 **Abstract**

10 This paper aims at deriving fire fragility curves for a prototype steel pipe-rack in an industrial plant
11 subjected to localised fires. In particular, starting from a reference case study, uncertainties related to
12 the structural capacity and the size of the localised fires caused by a hole in a tank or a hole in a pipe
13 are included in the analyses. Thus, the influence of uncertainties in the derivation of the fragility
14 functions was highlighted by comparing four sets of analyses in which both demand and capacity
15 uncertainties were progressively introduced. Moreover, alongside the cloud analysis (CA), the
16 suitability of the Multiple Stripe Analysis (MSA) to build relevant probabilistic fire demand models
17 was assessed. Fire fragility curves were derived by considering the interstorey drift ratio (ISDR) as
18 engineering demand parameter (EDP) and by assessing different relevant intensity measures (IMs)
19 that represent the severity of localised fires. It was found that by introducing uncertainties in the steel
20 yield strength, lower probabilities to exceed the life safety and the near collapse limit states with
21 respect to the reference case study were observed. Moreover, the inclusion of further uncertainties,
22 described with continuous physically-based probability functions of the size of the fire diameter,
23 affected the probabilistic models by lowering the probability of exceedance. These functions provide

24 a more realistic description of the fire scenario, enabling a better representation of the structural
25 vulnerability. For this case study, the CA exhibited better suitability for the derivation of fire fragility
26 curves than the MSA. All the analysis results are thoroughly discussed in the paper.

27 **Keywords**

28 Parameter uncertainties; Cloud analysis; Multiple Stripe analysis; Localised fires; Probabilistic fire
29 demand model; Steel pipe-rack structure

30 **1. Introduction**

31 Fire safety is a fundamental requirement of the design of civil and industrial structures, which
32 according to the current European norms [1] may be satisfied by employing either a prescriptive or a
33 performance-based approach. The prescriptive approach mainly consists in "deemed-to-satisfy"
34 solutions and employs nominal fire curves, e.g., ISO 834 or hydrocarbon curves, that do not represent
35 the real fire behaviour. Instead, Performance-Based Fire Engineering (PBF) provides performance
36 objectives and requirements to be satisfied and exploits more realistic fire curves, that consider the
37 fire characteristics and the environment in which the structure is located. In general, PBF allows for
38 a better description of the actual fire behaviour, an increase in design flexibility and a reduction of
39 the construction costs but, on the other hand, it entails an adequate expertise of the designer and the
40 employment of advanced tools, like numerical software for thermal and structural analyses or
41 probabilistic frameworks for the definition of plausible fire events or for fire risk assessment. Whilst
42 numerical simulation of several types of structures and resisting mechanisms in fire can rely on
43 thoroughly validated software and new developments, suited for the investigation of complex
44 phenomena [2-8], the extension of probabilistic concepts to fire safety engineering requires separate
45 studies addressing specific structural types, fire characteristics and scenarios. In this respect, fragility
46 functions/curves are useful tools for risk assessment, hazard mitigation and expected damage
47 estimation of structures and infrastructures, but their implementation in fire engineering is still at an
48 initial stage, in particular for industrial plants. As performance-based fire engineering and fully

49 probabilistic structural fire engineering approaches are arising in the design practice, the definition
50 of probabilistic fire demand models (PFDMs) and fire fragility curves is becoming important. Indeed,
51 despite meaningful indications of different nature can be obtained by applying the PBFEE with a
52 deterministic approach [9-14], a probabilistic approach provides more general considerations, as well
53 as useful tools, like fire fragility curves, which show the probability of exceedance of specific limit
54 states, defined according to appropriate engineering demand parameters (EDP), conditioned on a
55 suitable intensity measure (IM) that characterise the fire, such as the fire dimension or the fire load.
56 These curves may be integrated in a fully probabilistic structural fire engineering (PSFE) framework,
57 contributing, for instance, to estimate the expected damage of a structure when combined with
58 probabilities of occurrence of fires in a specific context, e.g. residential or industrial.

59 Though the probabilistic approach has been widely exploited in Performance-Based Earthquake
60 Engineering (PBEE) [15-20], there are only a few works focused on the development of fire fragility
61 curves [21-25]. Among the others, in [22, 23] a methodology for developing fire fragility curves for
62 steel structures exposed to compartment fires, relevant to office and dwelling buildings, was
63 presented. Lange et al. [24] and Shrivastava et al. [25] adapted the probabilistic framework of the
64 Pacific Earthquake Engineering Research Center (PEER) [26] to fire engineering. In addition,
65 methods to compute fragility curves were mainly deployed in the context of PBEE. For instance, the
66 three main methods used to build probabilistic demand models: cloud analysis (CA), incremental
67 dynamic analysis (IDA), and multiple stripe analysis (MSA), were compared in [15]. Shome et al.
68 [16] and Cornell et al. [17] laid the groundwork for the adoption of cloud analysis in seismic
69 applications. Baker [18] instead, investigated incremental dynamic analysis and multiple stripe
70 analysis and developed a fragility functions fitting based on a maximum likelihood estimation. Luco
71 and Cornell [19] described the concepts of efficiency and sufficiency of an IM to assess its suitability
72 for developing seismic fragility functions, while a relative measure between two IMs, i.e., relative
73 sufficiency, was proposed as alternative sufficiency indicator in [20].

74 Probabilistic fire analyses and fragility curves become even more rare when it comes to industrial and
75 petrochemical plants, though their piping systems mainly transport flammable material, liquid or gas
76 fuel. Natural or accidental events may severely damage the structure supporting the piping systems
77 [27-32], usually consisting of steel pipe-racks, and they may cause a release of flammable material
78 from a pipe or a tank. Although in general the probability of occurrence of a fire may be low, the
79 probability of ignition of the spilled flammable material increases in industrial environments and
80 severe consequences are expected, as shown, among the others, by Uehara [33], Chan and Lin [34],
81 Zheng and Chen [35] and Shu and Chong [36]. Therefore, the fire risk cannot be ignored for
82 petrochemical plants, and the definition of specific probabilistic fire demand models (PFDMs) is
83 desirable. For this purpose, plausible fire scenarios, representing pool fires resulting from leakage
84 and loss of containment from a pipe or a tank, should be defined. Methods to quantify the probability
85 of occurrence of a loss of fuel and the characteristics of the arising fires, e.g., the mass flow rate
86 resulting from a fuel leakage through a hole in a tank or in a pipe, were provided in [37-40]. These
87 methods introduce a variability in the fire characteristic, or in general in the fire demand, that should
88 be carefully considered when developing PFDMs. However, uncertainties may affect the capacity of
89 the structures as well. In this respect, Gernay et al. [22, 23] indicated several sources of uncertainties
90 that may influence the structural capacity of residential or office buildings, like the randomness in the
91 material properties and in the magnitude of the loads. Recently, a probabilistic model for the steel
92 properties at elevated temperature was illustrated in [41, 42].

93 In this context, this paper gives a novel contribution to the field by developing fire fragility curves
94 for a prototype steel pipe rack exposed to localised fires, considering both demand and capacity
95 uncertainties, that will be useful to apply in probabilistic frameworks to estimate the expected damage
96 and/or in fire risk assessment analyses. It investigates the effect of including different uncertainties
97 by increasing the number of uncertain parameters and finally provides fragility curves that are
98 representative of a more realistic description of the fire scenario and structural behaviour. In detail,
99 starting from a reference case study presented in [43], additional numerical analyses were performed,

100 first integrating randomness in the steel material properties at elevated temperature, and then
101 introducing variability of fire characteristics for both material loss from a hole in a tank or in a pipe
102 in the model. To evaluate the effects of demand and capacity uncertainties, the four different sets of
103 analyses were compared throughout the whole procedure that brought to the development of fire
104 fragility curves for three relevant IMs. Among the different IM, a scaled distance, based on concepts
105 employed to describe blast or explosion hazard and obtained as a simple function of the fire
106 parameters, is proposed to characterise the fire severity. Efficiency and relative sufficiency concepts
107 were used to determine the most suitable IMs and the employment of not only the CA but also of the
108 MSA for building the fragility curves was investigated. The numerical analyses were carried out with
109 the software SAFIR [2], since it enables both structural and thermal analyses, and includes the
110 LOCAFI model for localised fires. Indeed, numerous works have investigated the thermal radiation
111 emitted from hydrocarbon pool fires to propose fire models [44-50], but only recently an analytical
112 model for localised fire, namely LOCAFI, was developed and integrated in a software [51-55]. This
113 model quantifies the thermal impact of localised fires on vertical structural elements assuming that
114 the flame shape is conical and based on the Heskestad flame length and temperature correlations [46,
115 55].

116 The paper is organised as follows: in Section 2 the prototype steel pipe-rack is described along with
117 the fire scenarios and the uncertain parameters; Section 3 presents the probabilistic fire analysis and
118 the derivation of the fire fragility curves; finally, in Section 4 the conclusions and the future
119 perspectives are drawn.

120 **2. Description of a prototype steel pipe-rack subjected to localised fires**

121 In this section the prototype steel pipe-rack is presented, together with its numerical modelling.
122 Analogously, the pool fire scenarios and the associated localised fire models are described as well.
123 Finally, the probabilistic approach employed to account for uncertainties is outlined and the structure
124 of the numerical analyses is delineated. For comparison purposes, four case studies are defined

125 depending on the source of the uncertainties introduced in numerical simulation. Further details on
126 the structural and fire models adopted in the analyses can be found in [43].

127 The case study is based on an existing petrochemical plant located in Italy, whose seismic behaviour
128 was thoroughly studied [28-31], and it is composed of several steel frames with rigid beam-to-column
129 joints, pinned column-base joints in the transversal direction and vertical braces in the longitudinal
130 direction with repeated modules composed of seven bays and only one equipped with bracings. The
131 structural contribution of the piping system was neglected, and the geometry of the supporting steel
132 pipe rack was simplified, resulting in the case study depicted in Figure 1. A regular portion of the
133 structure was analysed, consisting of a six-bay module frame with a total extension of $L_s=36\text{m}$. The
134 vertical load due to the self-weight of the pipes and their content was assumed equal to $q_v=75\text{kN/m}$,
135 whilst a horizontal load $q_H=2\text{kN/m}$ was applied to take into account the friction of the pipes.
136 Moreover, point loads were applied at midspan of the longitudinal beams, i.e., $V=15\text{kN}$ vertical and
137 $H=7.5\text{kN}$ horizontal loads. As for the fire models later described in this paper, wind effects were
138 neglected and no wind loads were applied.

139 The numerical model was defined with the thermo-mechanical non-linear finite element software
140 SAFIR [2]. In detail, the model comprised HEA 340 columns, HEA 200 longitudinal beams, a lower
141 row of HEA 300 transversal beams and HEB 300 for the remaining transversal beams, all made of
142 S275 steel. 936 3D Bernoulli beam finite elements, having length of 50 cm each, were employed in
143 the analyses. Columns were pinned at their base in both principal directions, transversal beams were
144 end fixed to the columns, whilst the longitudinal beams were pinned to the columns (Figure 1b). Since
145 the heating of the longitudinal bracing system, based on the investigated fire scenarios, was very
146 limited and the major thermal impact occurred in the transverse direction, the bracing system was
147 substituted in the model with horizontal restraints in the longitudinal direction to limit the
148 computational burden.

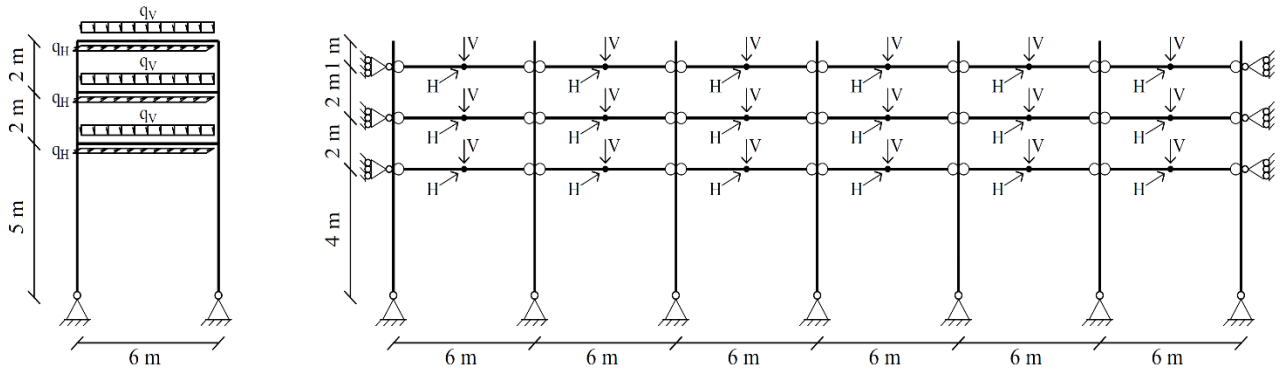


Figure 1. Case study

149

150 2.1. Fire scenarios description and localised fire models

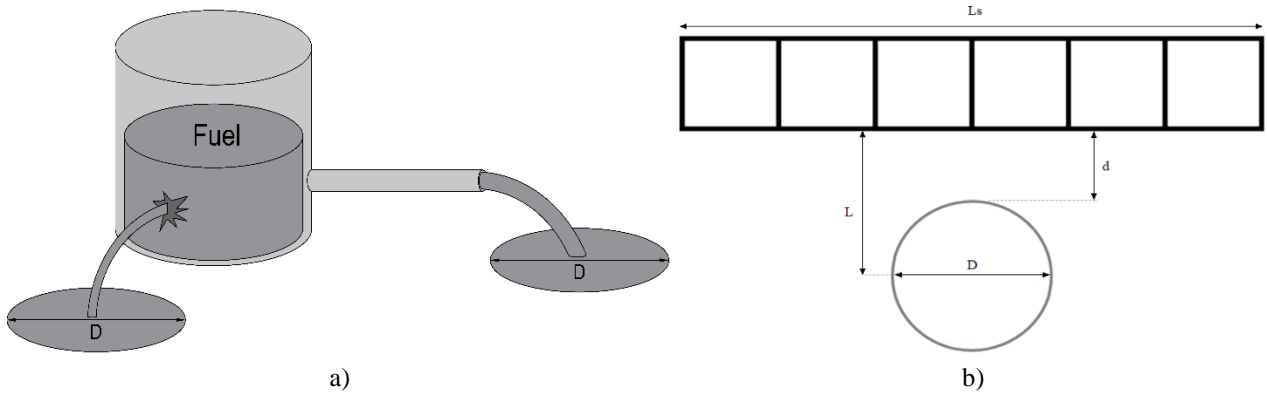
151 Fire scenarios consisting of pool fires resulting from a flammable material leakage or from a burning
 152 tank (Figure 2a) in industrial plants were investigated. A meaningful set of plausible localised fires
 153 impacting the structure with different levels of intensity, that cause from low consequences to the
 154 collapse of the entire structure, was considered. The set of scenarios was defined varying three
 155 parameters, i.e., the fuel type, the fire diameter D and the fire-structure distance d , where the latter is
 156 the distance separating the edge of the fire and the structure. As shown in Figure 2b, the fires were
 157 always located in front of the structure, with the fire centre aligned with the central transversal beam
 158 of the structure. The distance between the fire centre and the structure is indicated as L . The analyses
 159 performed in [43], used as reference in this work and referred to as Case Study 0 (CS0), were
 160 performed employing the pool fire parameters reported in Table 1. Such analyses were expanded in
 161 this work as described in Section 2.2.

162 **Table 1.** Set of pool fire scenarios – fuel, fire-structure distance d and fire diameter D values used in the reference analysis - CS0

Pool fire parameters		Number of analyses
Fuels	Pentane, Kerosene, Heptane, Gasoline, Fuel Oil, Benzene, Acetone	7
Distance d [m]	0.5, 1, 2, 3, 4, 5, 6	7
Diameter D [m]	5, 7.5, 10, 12.5, 15, 17.5, 20, 22.5, 25, 27.5, 30	11
Total number of analyses		539

163 In CS0 7 liquid fuels were selected for the definition of the fire scenarios, since petrochemical plants
 164 deal with various flammable products, as well as 7 fire-structure distances. Distances higher than 6
 165 m were not investigated since for $d=6$ m the selected fires were already having a limited impact on
 166 the structure. Eleven equally spaced diameters were considered, assuming a uniform distribution of

167 diameters in the 5 m to 30 m range, i.e., fires with diameters in the selected range all occur with the
 168 same probability, without distinguishing between leakage from a hole in the tank or from a pipe
 169 (Figure 2a). By varying the three parameters, 539 different localised fires were obtained and for each
 170 of them a thermo-mechanical analysis was performed, considering 60 minutes of thermal exposure.



171 **Figure 2.** a) Liquid outflow through a tank or a pipe; b) Fire-structure distance d and fire diameter D

172 A localised fire model integrated in SAFIR was employed to describe the fire development. Such
 173 model, i.e, LOCAFI model [55], belongs to the category of analytical models that exploit the virtual
 174 solid flame concept and was proven to provide accurate results, without being as demanding as more
 175 refined computational fluid dynamics (CFD) models. The model relies on the existing Heskestad
 176 correlations for localised fires included in Annex C of EN1991-2 [1] and describes a localised fire
 177 with a conical shape. It was validated against experimental data of fires characterised by diameters
 178 up to 50 m [55,56]. Localised fires are obtained in the model by defining the fire diameter D and the
 179 rate of heat release (RHR) Q of the fire. Indeed, additional information as the flame length L_f and
 180 temperature evolution along the flame axis can be derived from these two parameters

$$L_f = 0.0148Q^{0.40} - 1.02D \text{ [m]} \tag{1}$$

$$T(z) = 20 + 0.25Q_c^{\frac{2}{3}}(z - z_0)^{-\frac{5}{3}} \leq 900 \text{ [}^\circ\text{C]} \tag{1}$$

181 with

$$Q_c = 0.8Q \text{ [W]} \text{ and } z_0 = 0.00524Q^{0.40} - 1.02D \text{ [m]} \tag{2}$$

182 Where Q_c is the convective part of the rate of heat release Q and z_0 is the virtual origin of the fire
 183 source. The rate of heat release Q employed in the analyses was obtained as follows

$$Q = \dot{m}_b \Delta H_c \left(\frac{D\pi^2}{4} \right) \text{ [kW]} \quad (3)$$

$$\dot{m}_b = \dot{m}_\infty (1 - e^{-k\beta D}) \left[\frac{\text{kg}}{\text{m}^2\text{s}} \right]$$

184 where the mass burning rate \dot{m}_b was defined by Zabetakis and Burgess [58]. \dot{m}_∞ is the limiting mass
 185 burning rate, $k\beta$ is the empirical constant defined as the product between the extinction coefficient k
 186 and the mean beam length corrector β and ΔH_c is the heat of combustion (kJ/kg). The values
 187 employed in the analyses are reported in Table 2 [59]. For pentane the mass burning rate was taken
 188 as the limiting mass burning rate, and thus, no empirical constant is provided in Table 2. As a
 189 reference value to quantify the fuel intensity, the equivalent RHR density of the fuel q was obtained
 190 as follows

$$q = Q / \left(\frac{D\pi^2}{4} \right) \text{ [MW/m}^2\text{]}, \text{ with } \dot{m}_b = \dot{m}_\infty \quad (4)$$

191

Table 2. Fuel properties

Fuel	Limiting mass burning rate \dot{m}_∞ [kg/m ² s]	Empirical constant $k\beta$ [m ⁻¹]	Heat of combustion ΔH_c [kJ/kg]	Equivalent RHR density q [MW/m ²]
Acetone	0.038	2.24	25800	0.98
Fuel Oil	0.034	1.67	39700	1.35
Gasoline	0.055	1.48	43700	2.40
Kerosene	0.063	1.27	43000	2.71
Benzene	0.085	2.70	40100	3.41
Heptane	0.081	1.39	44600	3.61
Pentane	0.095	–	48800	4.64

192

2.2. Uncertainties in the structural and in the fire models

193 In CS0 [43] the variability of the fire input, or in general of the thermal demand, was accounted for
 194 by varying the parameters characterising the fire considering a predetermined set of values. However,
 195 a probabilistic approach, accounting also for uncertainties that may have a significant impact on the
 196 structural capacity, e.g., steel mechanical and thermal properties and the applied loads [22], should
 197 be preferred. In the specific case of the analysed pipe-rack, applied vertical loads are well defined in
 198 case of normal service conditions, meaning that no significant variation is foreseen. Conversely, the
 199 uncertainty related to the steel properties, and in particular to the mechanical properties, may

200 significantly affect the structural behaviour, as highlighted in [22,23]. Nevertheless, steel thermal
 201 properties have relatively low variances and the deterministic values from EN-1993-1-2 [57] can be
 202 taken [22]. Based on this discussion, in this work a probabilistic approach was adopted to consider
 203 uncertainties affecting both the fire demand and the structural capacity with reference to the yield
 204 strength at ambient and at elevated temperature. Starting from the reference case study CS0,
 205 uncertainties related to the steel yield strength were implemented in a new set of analyses, namely
 206 Case Study 1 (CS1). In detail, in CS0 the properties of steel at elevated temperature were taken as in
 207 EN 1993-1-2 [57], whilst the analyses summarised in Table 1 were run in CS1 by considering the
 208 logistic EC3-based probabilistic model proposed by Khorasani et al. [41] and Qureshi and al. [42] for
 209 the yield strength at elevated temperature, whereas the Young's modulus and the proportional limit
 210 were taken as in EN 1993-1-2 [57]. In this model the reduction of the yield strength at elevated
 211 temperature follows a probabilistic distribution, in which the variability of the value of the retention
 212 factor k_y , defined as the yield strength at a given temperature T measured at a 2% strain normalized
 213 by the yield strength at room temperature, is accounted for by means of the following equation

$$k_y = \frac{1.7 \exp[\text{logit}(\hat{k}_y^*) + 0.412 - 0.81 \cdot 10^{-3} \cdot T + 0.58 \cdot 10^{-6} \cdot T^{1.9} + 0.43\varepsilon]}{\exp[\text{logit}(\hat{k}_y^*) + 0.412 - 0.81 \cdot 10^{-3} \cdot T + 0.58 \cdot 10^{-6} \cdot T^{1.9} + 0.43\varepsilon] + 1} \quad (5)$$

214 where

$$\text{logit}(\hat{k}_y^*) = \ln\left(\frac{\hat{k}_y^*}{1-\hat{k}_y^*}\right), \hat{k}_y^* = \frac{k_{y,EN1993-1-2} + 10^{-6}}{1.7} \quad (6)$$

215 $k_{y,EN1993-1-2} = k_{y,EN1993-1-2}(T)$ is the retention factor of the yield strength at elevated temperature
 216 according to EN1993-1-2 [57] and ε is the standard normal distribution. The yield strength at ambient
 217 temperature also varies according to Eqs. (5) and (6) in terms of ε . Hence, the change in the steel
 218 strength with temperature was characterised by a different k_y reduction factor, determined according
 219 to Eq.(5) and values of ε generated with a Latin Hypercube sampling, in each one of the 539 analyses.
 220 Figure 3a illustrates the distributions of the retention factors k_y obtained at different temperatures,
 221 i.e. 20°C, 400°C and 600°C. It can be observed that the probabilistic model allows for higher retention

222 factors and in turn yield strengths, compared to the EN1993-1-2 until very high temperatures are
 223 reached. In detail, the 0.5 quantile of k_y is always higher than $k_{y,EN1993-1-2}$ for $T < 700^\circ\text{C}$, whilst the
 224 mean of k_y is higher than $k_{y,EN1993-1-2}$ until approximately 900°C . In particular, as reported in [60]
 225 the logistic model described in Eqs. (5) and (6) implicitly includes the effect of strain hardening at
 226 lower temperatures and therefore, k_y is higher than 1.0 at ambient temperature and consequently
 227 higher than $k_{y,EN1993-1-2}$.

228 Two further set of analyses, namely Case Study 2 (CS2) and Case Study 3 (CS3), were carried out to
 229 propose a more refined thermal demand model for which the fire diameter was computed with
 230 continuous physically-based probability distributions based on the leakage of flammable material
 231 from a hole in the tank or from a pipe. Indeed, in [43] the two probability density distributions were
 232 obtained by quantifying the liquid flow from a tank through a hole, or a pipe respectively. They were
 233 derived in order to determine the dimension of the fires that were most likely to occur and to be
 234 enough severe for the structure. For each of the two scenarios, consisting of 1000 different
 235 configurations, the fuels reported in Table 1 were considered and random tank and pipe geometries,
 236 hole dimensions and tank filling degrees varying within realistic ranges were selected. These analyses
 237 resulted in the fire diameter distributions depicted in Figure 3b. The illustrated normal distributions
 238 are defined with a mean of 20.39 m and a standard deviation of 14.75 m for a fuel leakage through a
 239 pipe and with a mean of 17.93 m and a standard deviation of 13.11 m for a fuel leakage through a
 240 hole. Therefore, the analyses of CS2 and CS3 were performed considering the diameter distributions
 241 for a liquid outflow from a pipe and from a hole, respectively. For each of the 49 fuel-distance pairs,
 242 11 diameters D were used from a set of 539 values picked with a Latin Hypercube sampling from the
 243 distributions. In Figure 3b also the distribution of the set of diameters employed in CS0 and CS1 is
 244 reported for comparison purposes. A summary of the quantities differentiating the 4 sets of analyses
 245 is provided in Table 3.

246

Table 3. Features of the investigated sets of analysis

Sets of analysis	Demand parameters Diameter D [m]	Capacity parameters Steel yield strength
------------------	---------------------------------------	---

CS0	Uniform distribution (Table 1 & Figure 3b)	Deterministic (EN 1993-1-2 [57])
CS1	Uniform distribution (Table 1 & Figure 3b)	Probabilistic (Eq. 1)
CS2	Probabilistic (Figure 3b – pipe)	Probabilistic (Eq. 1)
CS3	Probabilistic (Figure 3b – hole)	Probabilistic (Eq. 1)

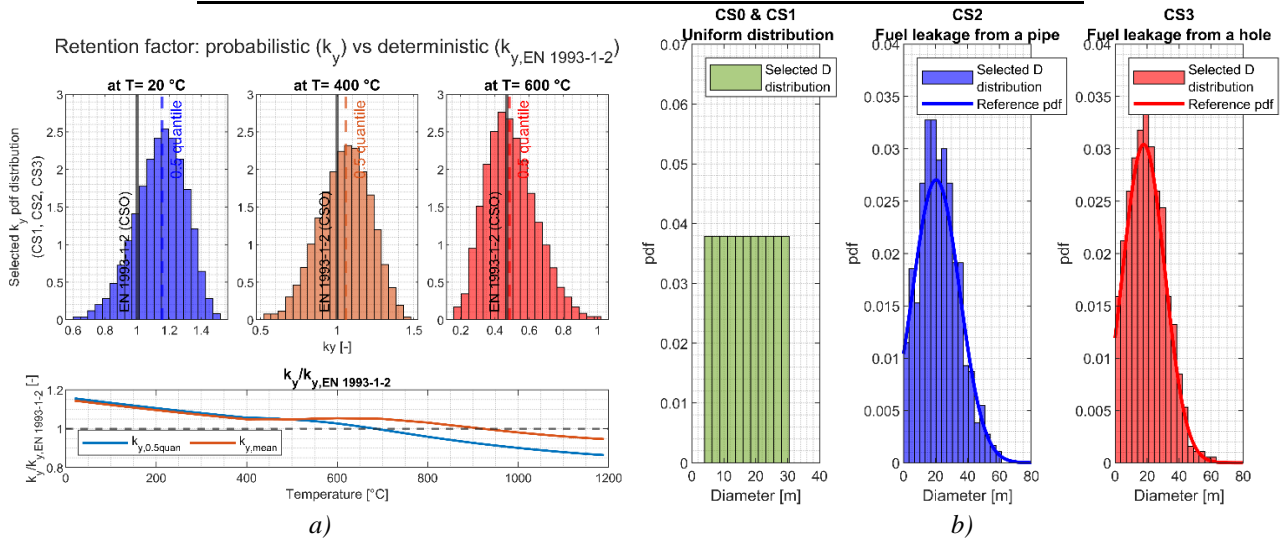


Figure 3. a) Probabilistic (Qureshi and al. [42]) vs deterministic retention factor model; b) Diameters distributions in CS0&CS1, CS2 and CS3

3. Probabilistic fire analysis

In this work, the results of numerical analyses are used to define a probabilistic fire demand model, with the aim to develop fire fragility curves, by providing a useful tool for practitioners that want to probabilistically assess or design a steel pipe-rack structure subjected to localised fires. Such curves describe the probability that an engineering demand parameter (EDP) exceeds a structural limit state (LS) conditioned on an intensity measure (IM).

$$P(\text{EDP} > \text{LS} | \text{IM}) \quad (7)$$

It is evident, that the selection of appropriate engineering demand parameters (EDP) and intensity measures (IMs) is crucial to propose fire fragility curves that accurately describe the structural response and the severity of the action. In this context, a significant data elaboration process had to be performed in order to only present the outcomes that provide a valuable information in terms of the selected EDPs and IMs. Therefore, in Section 3.1 and 3.2 suitable relevant IMs and EDPs are described.

261 **3.1.Intensity measures**

262 A good IM for a PFDM should be able to properly represent the severity of the fire scenario. In the
263 literature several IMs have been proposed for compartment fires, but their ability to characterise
264 localised fires is not guaranteed. Therefore, the 8 IMs reported in Table 4 are investigated. The first
265 7 were proposed by Randaxhe et al. [43], whereas the last one has been added in this work. Three
266 obvious choices for the IMs consisted in the 3 parameters characterising the fire scenarios, i.e., the
267 fire diameter D , the structure-fire distance d and the equivalent RHR density q . The latter is obtained
268 assuming that $\dot{m}_\infty = \dot{m}_b$, which is a good approximation for $D > 1$ m. The remaining IMs were
269 selected as functions of D , d and q . The fire position-diameter ratio was computed by considering the
270 distance between the structure and the fire centre L as $D/2+d$. Instead, Eq.(1) was employed in the
271 definition of the flame length L_f and the structure fire distance-flame length ratio d/L_f . HF_{avg} was
272 obtained by means of a weighted average of the heat fluxes HF on the four sides of the cross section
273 when it was impinged by the maximum radiative heat flux obtained with the LOCAFI model [55].
274 The RHR density q is typically employed as IM in applications for compartment fires [22-25], since
275 it provides an accurate estimate of the fire severity when a uniform fire distribution is assumed in an
276 entire compartment. However, the RHR density q cannot accurately describe the severity of fires
277 developing in a limited zone that might be far from the structure, i.e. localised fires. In particular, the
278 fire dimensions and the distance separating the structure and the fire might influence the heat flux
279 received from the structure and the number of critical elements that are severely heated.

280 In order to provide an indicator that considers these aspects and more accurately characterises the
281 severity of a localised fire, a further IM was defined, namely the scaled distance $d/A_{b,PE,eq}$ (Table 4).
282 As shown later in this paper, the scaled distance is one of the best IM candidates yet being much
283 simpler to derive than HF_{avg} and is obtained as the ratio between the structure-fire distance d and the
284 equivalent pentane surface $A_{b,PE,eq}$, computed as

$$A_{PE,eq} = \frac{Q}{\dot{m}_{b,PE}\Delta H_{c,PE}} = \frac{q(1 - e^{-k\beta D})\left(\frac{\pi D^2}{4}\right)}{\dot{m}_{b,PE}\Delta H_{c,PE}} \quad [m^2] \quad (8)$$

Where $\dot{m}_{b,PE}$ and $\Delta H_{c,PE}$ are the mass burning rate and the heat of combustion of pentane, respectively (Table 2). $A_{b,PE,eq}$ represents the equivalent surface of pentane to obtain the same RHR of the actual localised fire. Thus, the lower the scaled distance $d/A_{b,PE,eq}$ the higher the severity of the fire. It is worth to point out that in the development of fragility curves related to the blast or explosion hazard, a scaled distance is widely employed as IM, e.g. in [61-63], which is defined as the structure-explosion distance over a fractional power of an equivalent TNT mass M_{TNT} . Analogously to $A_{b,PE,eq}$ (Eq. (8)), M_{TNT} is obtained as the mass of TNT that is necessary to obtain the same energy released by the actual explosion.

Table 4. Investigated Intensity Measures (IM)

IM	Name	Function/Formula
D [m]	Fire diameter	f(D)
d [m]	Structure fire distance	f(d)
q [MW/m ²]	Equivalent RHR density of the fuel	f(q) = $\dot{m}_{\infty}\Delta H_c$
L/D	Fire position-Diameter ratio	f(D, d) = (D/2 + d)/D
L _f [m]	Flame length	f(D, q) = Eq. (1)
HF _{avg} [kW/m ²]	Maximum average heat flux impinging the structure	f(D, d, q) see [26]
d/L _f	Structure fire distance-Flame length ratio	f(D, d, q) = d/Eq. (1)
d/A _{b,PE,eq} [m ⁻¹]	Scaled distance	f(D, d, q) = d/Eq. (8)

3.2. Engineering demand parameters

The EDP should be a good indicator of the structural response, but an EDP suited for a particular case might not be the best choice for a different structure or for a different action (e.g., fire, seismic, impact, etc.). For instance, the maximum temperature and the vertical deflections of the structural members may be identified as relevant EDPs for steel buildings exposed to compartment fires but are not suited for the proposed case study. Indeed, since the structural members are not engulfed in fire, limited vertical deflections were registered and a single temperature measure cannot adequately represent the complex thermal distribution inside and along the structural members. Therefore, in [43] the

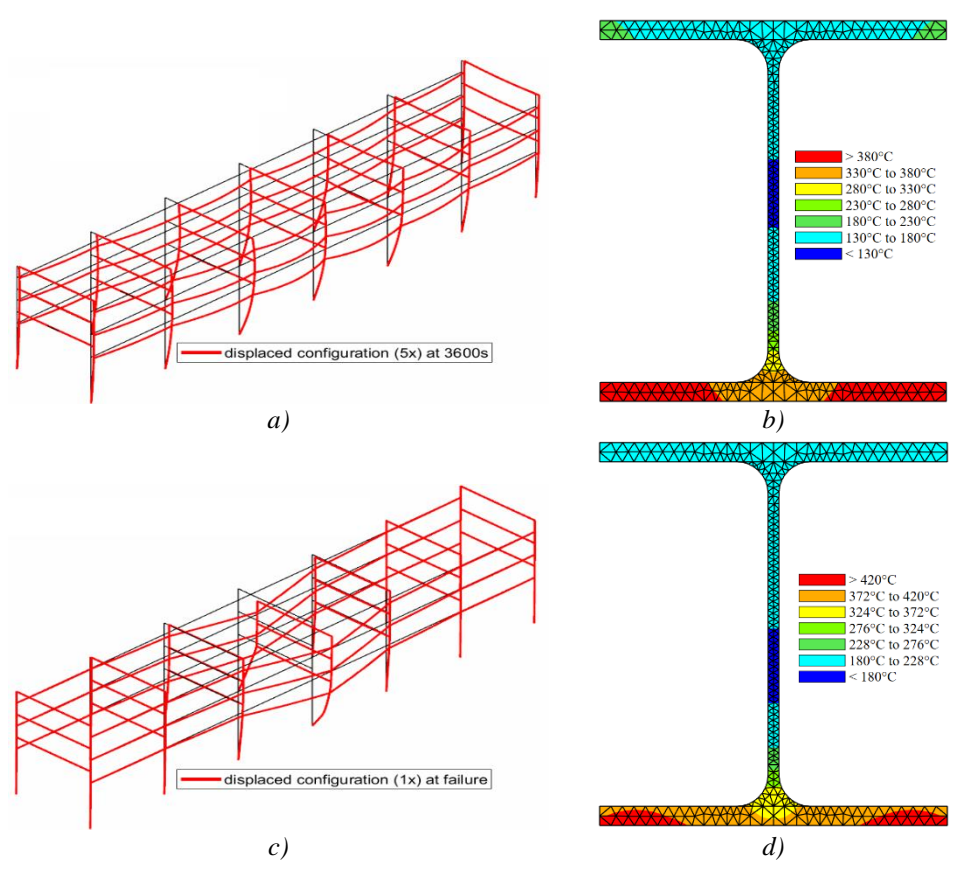
303 numerical results were examined thoroughly to identify an adequate EDP among different candidates,
304 e.g., the inter-storey drift ratio, the axial load and the bending moment in the structural elements, the
305 maximum average temperature within the whole structure and the average temperature within the
306 most stressed structural elements. Finally, the inter-storey drift ratio (ISDR) was selected as EDP
307 since it accurately represents the structural state regardless from the fire scenario and is widely
308 employed for other types of structures and actions, e.g., seismic actions. Indeed, despite in general
309 thermally induced drifts are not directly correlated to damage, in the investigated case study large
310 drifts were the major contributing cause of structural failure. Moreover, though localised fires may
311 induce differential ISDR at the same floor, numerical results showed that in this work the ISDR could
312 be associated with the damage of a significant part of the structure and thus, could be taken as an
313 indicator of the global structural response.

314 Detailed information on the values of ISDR associated to specific structural damage states (LS in Eq.
315 (7)) is available in literature. In this study, the ISDR values of 5% and 2.5% were adopted for near
316 collapse limit state and life safety limit state respectively, according to the indications for steel
317 moment resisting frames of the American seismic rehabilitation prestandard [64]. The selected limit
318 states refer to a situation in which a small increase of thermal and/or mechanical loads would lead the
319 structure to failure, i.e. near collapse, or to a situation in which the structure is in a significant
320 deformative state, but still has a margin of bearing capacity to support additional thermal and/or
321 mechanical loads, i.e., life safety.

322 **3.3. Results of the numerical analyses**

323 The results of the 2156 numerical analyses performed for the four case studies (i.e., 4 x 539 analyses)
324 are reported. If failure was not attained earlier, the analyses were stopped at 60 min, since by
325 preliminary checks it was found that thermal equilibrium was reached in the steel members after that
326 time. Figure 4a and Figure 4c show the typical deformed shape of the structure at failure and after 60
327 minutes, respectively. Figure 4 refers to CS3 and Figure 4a and Figure 4b depict the structure exposed

328 to a heptane fire at a distance of 2 m and a diameter of 25.4 m, whereas Figure 4c and Figure 4d show
 329 the case with a heptane fire but diameter equal to 11.0 m. As depicted, the typical failure mechanism
 330 of the structure consisted in the loss of stability of the central frame, which in most of the cases
 331 experienced the largest transversal deformations. Despite the maximum displacements occurred at
 332 the top of the structure, the highest inter-storey drift ratios (ISDR) were registered in the transverse
 333 direction at the first level of the columns, i.e, at a height of 5m. Since no load increments were applied,
 334 the progressive increase of the transversal displacements was related to the effects of the fire
 335 exposure. Indeed, strength and stiffness degradation of steel occurred and consequently the load-
 336 bearing capacity of the structural members decreased. In addition, the structural members were
 337 partially restrained; thus, axial dilatation and thermal bowing of the members induced variations of
 338 the internal forces. In particular, thermal bowing in the columns was substantial due to the significant
 339 non-uniform temperature distributions in the cross sections and entailed an increase in second order
 340 effect importance, as depicted in Figure 4b and Figure 4d for the central column of the closest row to
 341 fire at a height of 5m.



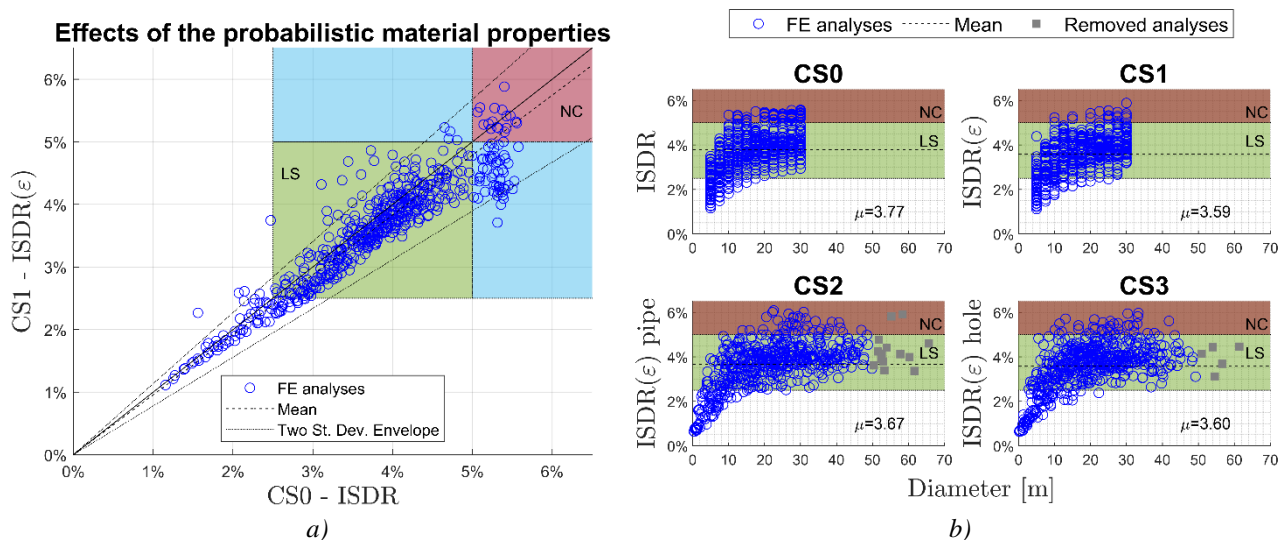
342 **Figure 4.** CS3 – Fuel=Heptane, d=2m: a) D=25.4m, deformed shape at failure; b) D=25.4m, temperatures of the front
343 row central column at 5m at failure; c) D=11.0m, deformed shape after 60 minutes; d) D=11.0m, temperatures of the
344 front row central column at 5m after 60 minutes

345 The maximum inter-storey drifts obtained in the analyses are represented in Figure 5 and Figure 6
346 and they are denoted as ISDR for CS0, and as $ISDR(\varepsilon)$ for CS1-CS3, where the steel yield strength
347 at elevated temperature varied in accordance with the standard normal distribution ε in Eq.(5). The
348 regions relevant to the life safety limit state and the near collapse limit states are indicated in green
349 ($2.5\% \leq ISDR < 5\%$) and in red ($ISDR \geq 5\%$).

350 The effects of the introduction of the variability in the steel material properties can be discussed
351 observing the comparison between ISDR from CS0 and CS1 proposed in Figure 5a. A good
352 correlation is found between the results of the two analyses (mean and standard deviation of the ISDR
353 are 0.96% and 0.09% respectively), but accounting for the steel yield strength uncertainties tends to
354 reduce the ISDR in CS1. The points inside the green and red shaded areas represent the analyses
355 exceeding both the life safety and the near collapse limit state for each single analysis of the two sets,
356 i.e. CS0 and CS1. Instead, the points lying inside the blue areas are associated with the analyses for
357 which the near collapse limit state was exceeded in one CS, but only the life safety limit state was
358 reached for the other CS. In this respect, the CS0 deterministic material property assumptions appear
359 more severe since analyses that exceed the near collapse for CS0 are, conversely, in many cases still
360 only exceeding the life safety limit state for CS1. Indeed, in CS1 the steel retention factors of the
361 yield strength are on average larger than the one prescribed in the EN 1993-1-2 and used in CS0 (see
362 the 0.5 quantile and the mean of the picked k_y factors in Figure 3). Thus, higher strength is exhibited
363 in the CS1 analyses. This holds true when the ISDR of CS0 are compared to the ones of CS2 and CS3
364 as also in these cases the probabilistic material model was considered, as shown in Figure 5b. In
365 addition, the mean ISDRs of CS1, CS2 and CS3, i.e., 3.59%, 3.67%, 3.60%, reflect the mean of the
366 diameter distributions employed in such analyses, i.e., 17.5m, 20.39m, 17.93m. Larger diameters
367 entail more severe fires, leading to higher values of ISDR.

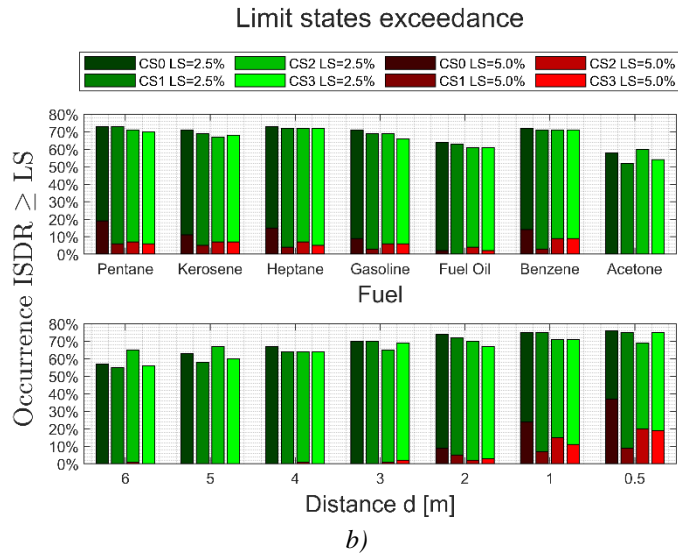
368 To better understand the effects of uncertainties, the results of each of the analyses performed for
369 CS2 and CS3 were examined. As mentioned before, since the LOCAFI model was not extensively

370 investigated for fire diameters larger than 50 m ($D > 50$ m) [55,56], the analyses obtained for diameters
 371 larger than 50 m in CS2 (14 analyses) and in CS3 (5 analyses) are explicitly indicated in Figure 5b
 372 with grey squares and are not considered later in the development of the PFDMs. Besides, it has to
 373 be observed that some analyses experienced $ISDR > 5\%$ without showing structural failure owing to
 374 lack of numerical convergence caused mainly by material fracture occurred in a highly deformed
 375 configuration, that also determined runaway in some analyses. Therefore, the analyses run until the
 376 end (60 minutes). For such analyses it was checked that by slightly increasing the loads, failure was
 377 reached to confirm that they were in a near collapse state.



378 **Figure 5.** Influence on the ISDR: a) of the uncertainties in the material properties; b) of the uncertainties in the material
 379 properties and the diameter distribution

380 Finally, as shown in Figure 6, the near collapse limit state threshold (5%) was exceeded more
 381 frequently in CS0, whilst the 2.5% threshold exceedance occurred for all four case studies in a
 382 comparable number of analyses for a given fuel or structure-fire distance. Again, the trend of the
 383 results indicates that higher ISDR may be reached for the same fire scenario when the deterministic
 384 material properties are employed (CS0), for which plasticity and load redistribution occur for lower
 385 load levels or fire intensity compared to the case studies with the probabilistic material model (CS1-
 386 CS3).



387 **Figure 6.** a) LS thresholds exceedance for type of fuel and for distance d

388 **3.4.Cloud analysis and Multiple stripe analysis**

389 Though numerous probabilistic seismic demand models (PSDM) are available, the literature is
 390 currently lacking extensive applications in the fire context and only few probabilistic fire demand
 391 models (PFDM) can be found [21-25]. With respect to PSDM, incremental dynamic analysis (IDA),
 392 Cloud analysis (CA) and Multiple stripe analysis (MSA) are usually employed to obtain fragility
 393 curves. PSDMs are obtained with IDA by incrementing an IM in dynamic analyses until the EDP
 394 exceeds a certain limit state (LS). However, scaling fire IMs, such as fire load or heat flux, can rapidly
 395 lead to unrealistic fire scenarios and thus, IDA is not well suited for a PFDM and is not applied in
 396 this work. Instead, both CA, also employed in [43] and MSA are proposed to develop the PFDM.

397 **3.4.1. Cloud Analysis (CA)**

398 Cloud analysis (CA) is suited to build a PSDM from EDP-IM pairs arranged in a data cloud. This
 399 procedure is particularly convenient as it does not require to perform several analyses for discrete
 400 quantities of IM as in MSA and thus, it is not necessary to determine the IM to be employed in the
 401 PSDM model a priori. This allows for the selection of the most suitable IM a posteriori, i.e., in light
 402 of the results of the numerical analyses and of the CA.

403 The CA method assumes that an EDP follows a lognormal distribution when conditioned on an IM.
 404 Hence, the probabilistic demand model can be characterised as follows

$$\widehat{\text{EDP}} = a\text{IM}^b \quad (9)$$

$$\ln(\widehat{\text{EDP}}) = A + B \ln(\text{IM})$$

405 where $\widehat{\text{EDP}}$ is the median of the EDP, and the parameters $a = \exp(A)$ and $b = B$ are identified by
 406 means of a linear regression. Indeed, the conditional median of the EDP given the IM is linear in the
 407 log–log space, whereas the conditional dispersion of the EDP given the IM is constant. Such
 408 dispersion, referred to as $\beta_{\text{EDP}|\text{IM}}$, can be determined as the standard deviation of the linear regression
 409 $\sigma_{\ln(\text{EDP})|\text{IM}}$

$$\beta_{\text{EDP}|\text{IM}} = \sigma_{\ln(\text{EDP})|\text{IM}} = \sqrt{\frac{\sum_{i=1}^n [\ln(\text{EDP}_i) - \ln(\widehat{\text{EDP}}_i)]^2}{n - 2}} \quad (10)$$

410 Finally, the fragility function can be defined in the form of a lognormal cumulative distribution
 411 function [42]

$$P(\text{EDP} > \text{LS}|\text{IM}) = 1 - \Phi\left(\frac{\ln\left(\frac{\text{LS}}{a\text{IM}^b}\right)}{\beta_{\text{EDP}|\text{IM}}}\right) \quad (11)$$

412 **3.4.2. Multi Stripe Analysis (MSA)**

413 MSA can be applied to build a demand model by considering a discrete set of IMs, so that EDP-IM
 414 pairs are arranged in a stripe for each IM level. However, a minimum number of analyses should be
 415 performed for each level of IMs to obtain meaningful models [15]. In the framework of this work,
 416 MSA analysis was employed for IMs and CSs that allowed for stripes with at least 7 occurrences, i.e.,
 417 at least 7 analyses were performed for each value of the IM. Though at least 10 instances per stripe
 418 are usually suggested [15], the threshold was lowered to 7 to test the ability of MSA to provide
 419 efficient PFDMs with only few results for each IM level.

420 MSA is based on the definition of fraction of collapses for a predefined LS and for each i-th level of
 421 IM, i.e., for each stripe. Such fraction is obtained dividing the number k_i of analyses in which $EDP >$
 422 LS by the total number of analyses performed. Assuming that observations of “collapse” or “no-
 423 collapse” are independent for the different fire scenarios, a binomial distribution can be used to
 424 express the probability of observing k_i collapses among n_i fire scenarios given an IM_i

$$P(k_i \text{ collapses in } n_i \text{ fire scenarios}) = \binom{n_i}{k_i} p_i^{k_i} (1 - p_i)^{n_i - k_i} \quad (12)$$

425 where p_i is the probability to observe a collapse C given an IM_i . Such probability can be defined with
 426 a lognormal cumulative distribution function [18]

$$p_i = P_i(C|IM_i) = \Phi\left(\frac{\ln\left(\frac{IM_i}{\theta}\right)}{\beta}\right) \quad (13)$$

427 The function $\Phi(\)$ is the standard normal cumulative distribution function, while θ and β define the
 428 shape of the fragility function and are the median of the fragility function, i.e., the IM level generating
 429 a probability of exceedance of 50%, and the standard deviation of $\ln(IM)$, respectively. The parameter
 430 β is the dispersion of the fragility function and must not be confused with the term $\beta_{EDP|IM}$ in Eq.
 431 (10), which is the dispersion of the EDP conditioned on IM. In this work the fragility function is built
 432 with the maximum likelihood method, which aims at finding the probability distribution with the
 433 highest likelihood of having produced the fraction of collapse observed for each IM_i . The likelihood
 434 is defined as the product of the binomial probabilities

$$\begin{aligned} \text{Likelihood} &= \prod_{i=1}^m \binom{n_i}{k_i} p_i^{k_i} (1 - p_i)^{n_i - k_i} \\ \text{Likelihood} &= \prod_{i=1}^m \binom{n_i}{k_i} \Phi\left(\frac{\ln\left(\frac{IM_i}{\theta}\right)}{\beta}\right)^{k_i} \left(1 - \Phi\left(\frac{\ln\left(\frac{IM_i}{\theta}\right)}{\beta}\right)\right)^{n_i - k_i} \end{aligned} \quad (14)$$

435 where m is the number of IM levels or stripes. The optimal parameters $\hat{\theta}$ and $\hat{\beta}$ of the fragility function
 436 are obtained by maximising the likelihood as follows

$$\{\hat{\theta}, \hat{\beta}\} = \max_{\theta, \beta} \sum_{i=1}^m \left[\ln \binom{n_i}{k_i} + k_i \ln \Phi \left(\frac{\ln \left(\frac{IM_i}{\theta} \right)}{\beta} \right) + (n_i - k_i) \ln \left(1 - \Phi \left(\frac{\ln \left(\frac{IM_i}{\theta} \right)}{\beta} \right) \right) \right] \quad (15)$$

437 Once the optimal parameters are defined, the fragility function can be obtained employing the
 438 distribution assumed earlier (Eq.(13))

$$P(\text{EDP} > \text{LS} | \text{IM}) = \Phi \left(\frac{\ln \left(\frac{IM}{\hat{\theta}} \right)}{\hat{\beta}} \right) \quad (16)$$

439 The dispersion of the EDP conditioned on the IM for the i-th stripe $\beta_{\text{EDP}_i | \text{IM}_i}$ can be taken as in [25].

$$\beta_{\text{EDP}_i | \text{IM}_i} = \frac{\sigma_{\text{EDP}_i | \text{IM}_i}}{\mu_{\text{EDP}_i | \text{IM}_i}} \quad (17)$$

$$\sigma_{\text{EDP}_i | \text{IM}_i} = \sqrt{\frac{\sum_{i=1}^o [\text{EDP}_{i,o} - \mu_{\text{EDP}_i | \text{IM}_i}]^2}{n}} \quad \mu_{\text{EDP}_i | \text{IM}_i} = \frac{\sum_{i=1}^o \text{EDP}_{i,o}}{n} \quad \text{with } o = \text{occurrences at } \text{IM}_i$$

440 3.5.CA and MSA results

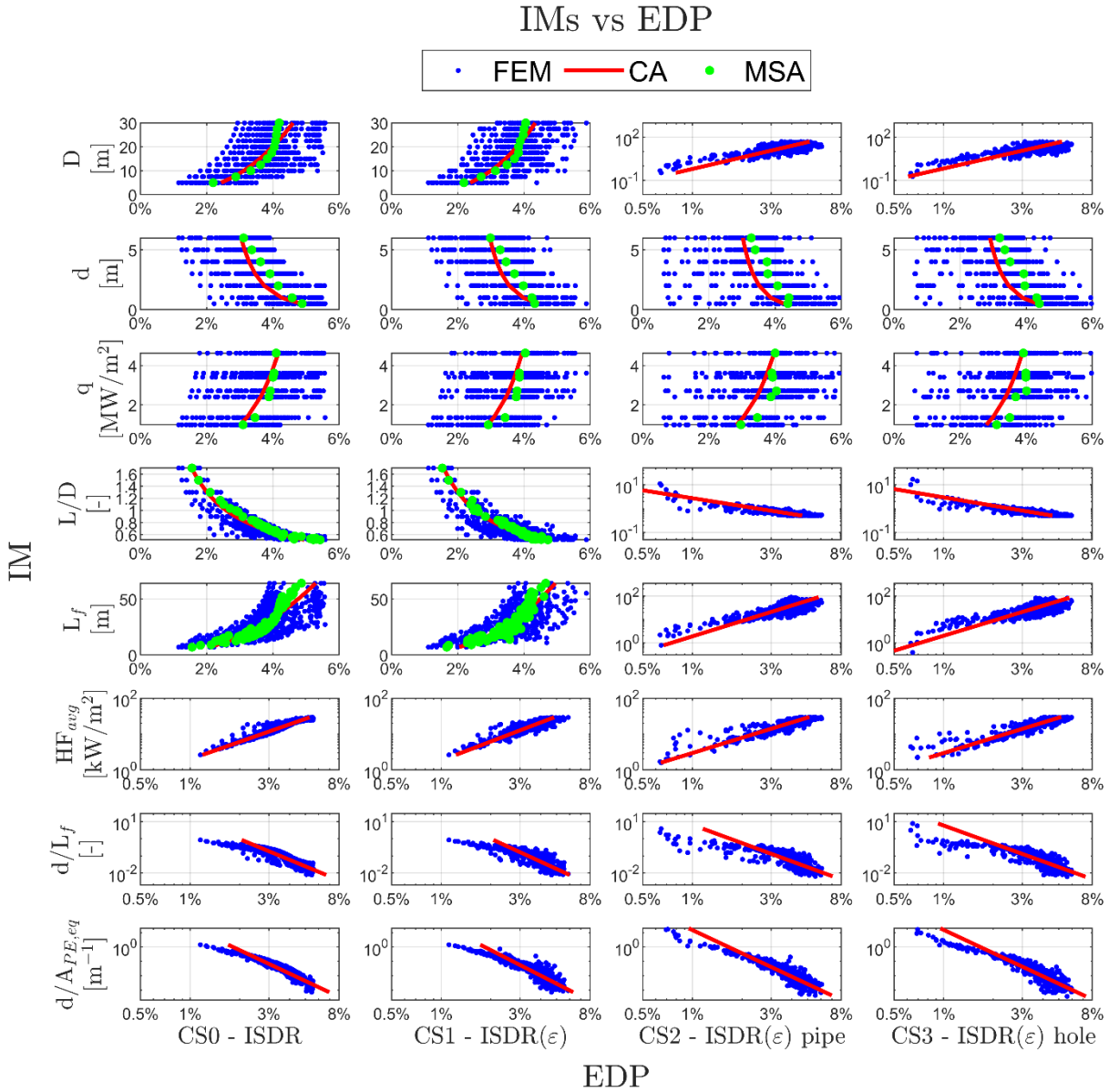
441 In order to derive the fire fragility curves, the results of the four case studies were analysed by means
 442 of CA and MSA. The ISDR was used as unique EDP and the IMs given in Table 4 were exploited.
 443 The CA was applied to all cases and all IMs, as mentioned in Section 3.4, whilst the MSA was
 444 employed only when at least 7 instances per stripe were available. As a result, the MSA was applied
 445 to CS0 and CS1 for IMs consisting of single fire parameters or simple functions of them, i.e., D, d, q,
 446 L/D and L_f ; while, due to the variability of the diameters D introduced in the analyses, MSA was used
 447 only for d and q in CS2 and CS3. Indeed, it appears that obtaining well-defined stripes is not trivial
 448 when uncertainties are included into the demand model as continuous probabilistic density functions.
 449 The obtained PFDMs are shown against the numerical results in an EDP-IM space in Figure 7. The
 450 CA regression is represented as a continuous line, while single points are used for each stripe of the
 451 MSA. A log-log space representation is preferred to better show the linear regression fit when only
 452 the CA is available. The parameters of the CA and the MSA defined in Sections 3.4.1 and 3.4.2 are
 453 reported in Table 5 and Table 6, respectively.

Table 5. Cloud analysis parameters

CA parameters								
IM	CS0		CS1		CS2		CS3	
	<i>a</i>	<i>b</i>	<i>a</i>	<i>b</i>	<i>a</i>	<i>b</i>	<i>a</i>	<i>b</i>
D	0.014	0.355	0.014	0.336	0.012	0.373	0.012	0.384
d	0.043	-0.188	0.040	-0.163	0.039	-0.138	0.039	-0.162
q	0.030	0.210	0.029	0.199	0.028	0.218	0.028	0.212
L/D	0.026	-0.975	0.025	-0.902	0.025	-0.912	0.026	-0.864
L _f	0.009	0.422	0.009	0.399	0.008	0.457	0.007	0.469
HFavg	0.007	0.620	0.007	0.569	0.005	0.706	0.005	0.708
d/L _f	0.020	-0.251	0.020	-0.227	0.017	-0.284	0.017	-0.289
d/A _{b,PE,eq}	0.018	-0.185	0.018	-0.170	0.017	-0.185	0.017	-0.186

Table 6. Multiple stripe analysis parameters

MSA parameters									
IM		CS0		CS1		CS2		CS3	
		$\hat{\theta}$	$\hat{\beta}$	$\hat{\theta}$	$\hat{\beta}$	$\hat{\theta}$	$\hat{\beta}$	$\hat{\theta}$	$\hat{\beta}$
Life safety limit state	D	5.911	0.461	6.209	0.550	-	-	-	-
	d	17.601	1.401	15.627	1.474	4748.121	6.707	26.229	2.125
	q	0.323	1.523	0.465	1.367	0.249	1.948	0.409	1.598
	L/D	1.071	0.189	1.034	0.214	-	-	-	-
LS=2.5%	L _f	12.046	0.319	12.882	0.338	-	-	-	-
	D	43.435	0.750	138.181	1.137	-	-	-	-
Near collapse limit state	d	0.500	0.923	0.107	1.496	0.248	1.227	0.254	1.143
	q	7.954	0.920	21.924	1.151	49.972	2.011	34.131	1.676
	L/D	0.541	0.056	0.466	0.133	-	-	-	-
LS=5.0%	L _f	58.685	0.489	121.218	0.719	-	-	-	-



456

Figure 7. Cloud and multi-stripe analysis fit models

457

Not all IMs allow for equally well-defined PFDMs and the dispersion of the EDP conditioned on IM

458

$\beta_{EDP|IM}$ provides a quantitative measure of the variations between the actual and the predicted EDP

459

values for a given IM. Such dispersions are summarised in Figure 8 for all the derived PFDMs. When

460

the MSA was used, dispersion values were determined according to Eq. (17) at each IM level. As

461

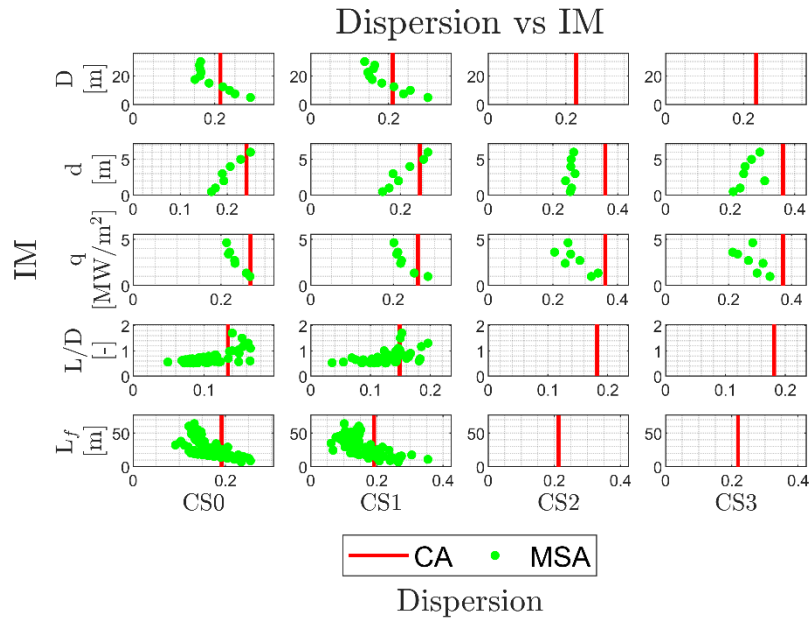
expected, the MSA applied with L/D and L_f as IMs, showed the highest variability in the dispersion

462

because only 7 analyses per stripe were used, confirming that at least 10 analyses for each IM level

463

[15] are probably necessary to obtain efficient demand models.



464 **Figure 8.** Cloud vs multi-stripe analysis dispersions

465 In fact, the dispersion is a good indicator to evaluate the efficiency of an IMs. An IM is efficient if it
 466 generates low $\beta_{EDP|IM}$ values, usually below 0.3 [15]. Therefore, the dispersion of the CA was
 467 employed to select the best IM candidates for developing the fire fragility curves. Dispersions were
 468 compared in the efficiency plot of Figure 9a, from which it can be observed that for CS2 and CS3 q
 469 and d , which are the only IMs completely independent from the diameter D (Table 4), cannot be
 470 deemed efficient. This is due to the fact that the fire diameter D is a fundamental parameter to
 471 characterise the fire severity and this is even more true when a probabilistic distribution of D is
 472 assumed as in CS2 and CS3. Nevertheless, even though for CS0 and CS1 q and d can be considered
 473 efficient, they show the highest dispersion values among the different IM. Based on this discussion,
 474 q and d were discarded and among the remaining IM candidates, the three with the highest efficiency
 475 were selected, namely L/D , HF_{avg} and $d/A_{b,PE,eq}$.

476 Besides, the sufficiency of the IMs was investigated to ensure an accurate estimate of the probability
 477 of a structural response given an IM, i.e., $P(EDP|IM)$. According to Luco and Cornell [19], IMs are
 478 sufficient when the structural response to a demand shows no trend in the correlation with the
 479 parameters defining such demand. However, the IMs candidates employed in this work were defined
 480 as functions of the fire parameters, i.e., D , d and q , and correlation was always observed between the
 481 residuals of EDP and these parameters. In this situation, a more appropriate sufficiency measure is

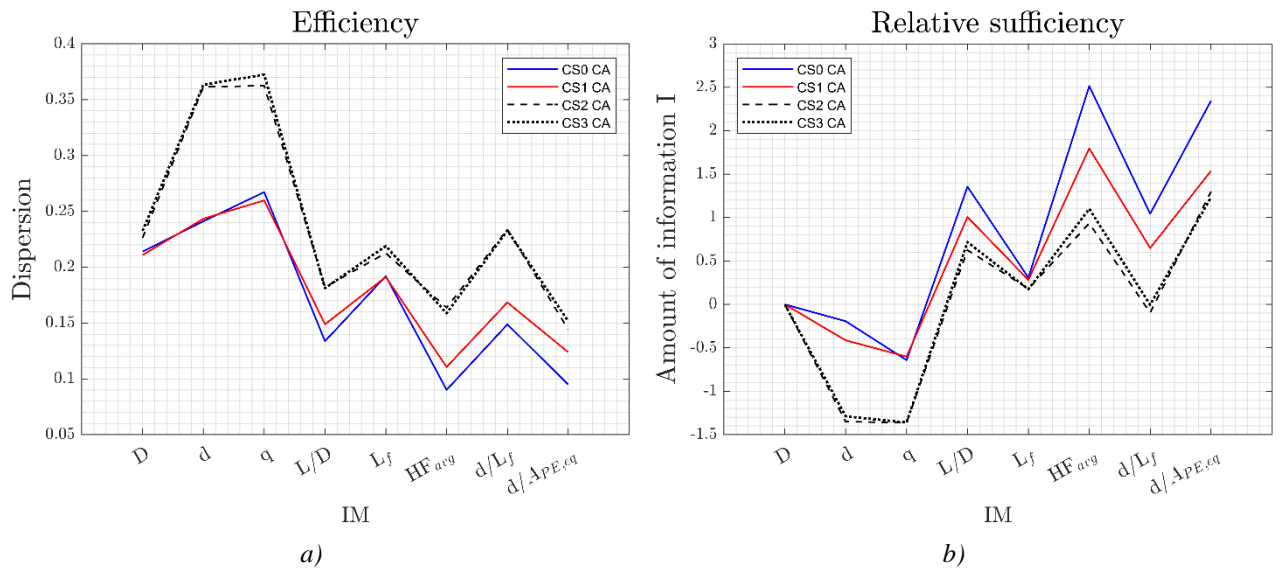
482 the relative sufficiency, which compares the sufficiency of IMs by evaluating the amount of
 483 information gained on average about the structural response. The amount of information I gained by
 484 IM_2 with respect to IM_1 can be evaluated according to [20]

$$I(\text{EDP}|IM_2|IM_1) \approx \frac{1}{n} \sum_{i=1}^n \log_2 \frac{p[\text{EDP} = \text{EDP}_i|IM_2]}{p[\text{EDP} = \text{EDP}_i|IM_1]}$$

$$P(\text{EDP} = \text{EDP}_i|IM) = \frac{1}{\beta_{\text{EDP}|IM} \text{EDP}_i} \Phi \left(\frac{\ln \left(\frac{\text{EDP}_i}{a IM_i^b} \right)}{\beta_{\text{EDP}|IM}} \right) \quad (18)$$

485 and is expressed in unit of bits of information. EDP_i is the parameter evaluating the structural response
 486 (ISDR) for each of the n fire scenarios, $P(\text{EDP}|IM)$ is the probability of a structural response given
 487 the IM and $\Phi(\cdot)$ is the standard gaussian probability density function. An IM is more sufficient than
 488 another if it provides more information on the structural response. It follows that IM_2 is more
 489 sufficient than IM_1 for positive values of $I(\text{EDP}|IM_2|IM_1)$. The higher the value of $I(\text{EDP}|IM_i|IM_1)$,
 490 the more sufficient the IM_i is. A relative sufficiency plot is depicted in Figure 9b, by comparing the
 491 amount of information I of the candidates IMs with respect to the diameter ($IM_1=D$). The choice of
 492 the reference IM is arbitrary, since selecting a different IM the relative sufficiency plot translates
 493 vertically, but the difference between the values of I for each IM remain unchanged. The three best
 494 IMs in terms of relative sufficiency are the same as for the efficiency and thus, no further
 495 consideration was necessary to choose the IMs for developing the fragility curves. For all the four
 496 sets of analyses $d/A_{b,PE,eq}$ permits for dispersions and amounts of information comparable with the
 497 ones obtained considering HF_{avg} as IM. However, $d/A_{b,PE,eq}$ has the advantage of being much more
 498 straightforward to calculate than HF_{avg} . As expected, Figure 9 shows that IMs are less efficient and
 499 less sufficient when uncertainties are introduced, but their ranking remains unchanged. Moreover,
 500 being d and q completely independent from the diameter D , their relative sufficiency is significantly
 501 worse when probabilistic distributions of the diameter are used (CS2 and CS3) and the diameter

502 provides more relevant information to characterise the fire severity, and in turn the structural
 503 response.



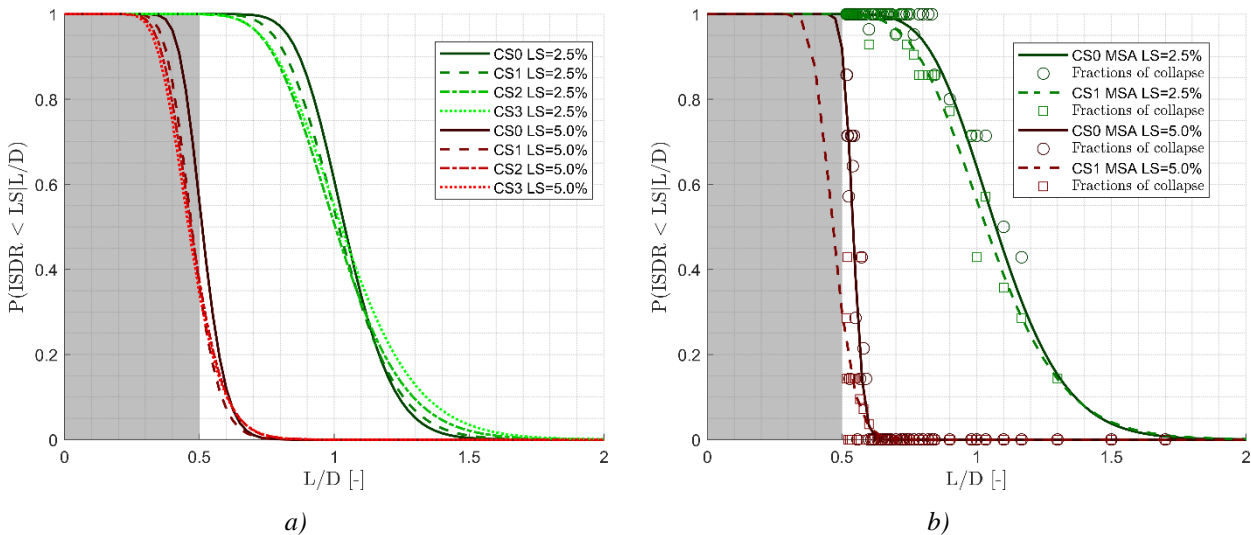
504 **Figure 9.** a) Efficiency and b) relative sufficiency of IMs

505 3.6. Fire fragility curves

506 Fire fragility curves were derived from the PFDMs obtained for each of the IM candidates given in
 507 Table 4. However, only the fragility curves obtained for the three most efficient and sufficient IMs
 508 are shown and discussed. The proposed curves can be used to quantify the probability that a steel
 509 pipe-rack exposed to a localised fire exceeds a predetermined limit state. The curves are developed
 510 for two limit states, namely the near collapse limit state and life safety limit state, for which a 5% and
 511 a 2.5% threshold is set on the ISDR. Fragility curves were derived for all the case studies, i.e. CS0,
 512 CS1, CS2 and CS3.

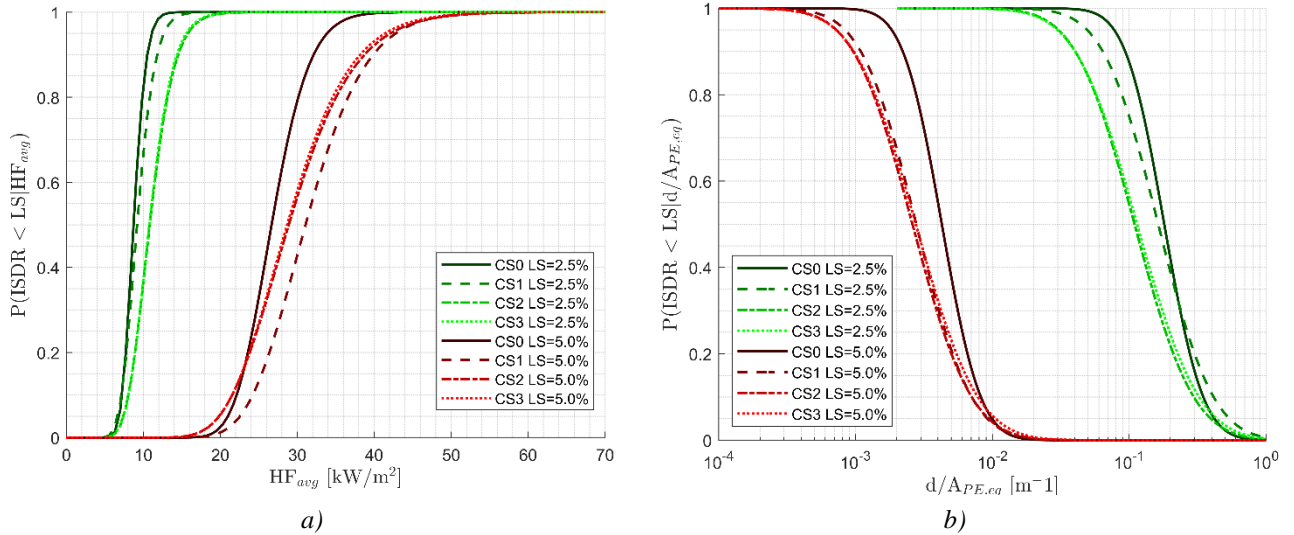
513 Figure 10 shows the fragility curves for the PFDM based on L/D as IM. A limitation should be applied
 514 to this model since for $L/D < 0.5$ part of the structure would be engulfed into the localised fire and a
 515 different structural response is expected, with the ISDR no longer being the most appropriate EDP.
 516 Therefore, these curves may not be suited for the range shaded in grey. All the fragility curves for a
 517 given limit state attain the median of the probability distribution, i.e., $P(\text{ISDR} > \text{LS} | L/D) = 50\%$ at
 518 similar ISDR values. For the life safety limit state the 50% probability is exceeded for
 519 $0.45 < L/D < 0.52$, while for the near collapse limit state this occurs for $1.03 < L/D < 1.06$. As expected,

520 here and in all the subsequent figures, the fragility curves show a higher dispersion when the
521 parameter uncertainties are incorporated, i.e. CS1, CS2, CS3.
522 For L/D fire fragility curves for CS0 and CS1 are obtained also from the MSA, as illustrated in Figure
523 10b. The fragility curves based on the MSA fit the fraction of collapses, intended as the ratio between
524 the cases in which a limit state was exceeded over the total number of fire scenarios (539) given an
525 IM_i . Though the IM ranges relevant to collapses are similar to the ones from CA, different values of
526 probabilities of exceedance are found. For instance, a higher curve is derived for the near collapse in
527 CS0, for which at $L/D=0.5$ the probability of exceedance is higher than 90%. Conversely, by
528 comparing the CS1 case study at the near collapse limit state the MSA and the CA provide similar
529 fragility curves. This was also observed at the life safety limit state for which good agreement between
530 the two methods to derive fragility curves is shown in Figure 10. However, since only few data were
531 available for each stripe (7 or 14) and the curve fit rather disperse fraction of collapses, the MSA
532 based fragility curves are deemed less reliable and the use of CA is suggested when less than 10 data
533 are available for each IM level, as recommended in [15].



534 **Figure 10** fragility curves for near collapse and life safety preventions with L/D as IM. a) CA; b) MSA
535 A significant improvement in efficiency and relative sufficiency was obtained by employing HF_{avg}
536 and $d/A_{b,PE,eq}$, whose associated CA based fragility curves are depicted in Figure 11a and Figure
537 11b, respectively. In Figure 11a, the probability of exceeding the life safety and the near collapse
538 limit states surpasses the 50% for $8.7 < HF_{avg} < 10.8 \text{ kW/m}^2$ and $26.6 < HF_{avg} < 31.1 \text{ kW/m}^2$ respectively.

539 For $IM=d/A_{b,PE,eq}$, the probability of exceeding the life safety and the near collapse limit states
 540 attains the 50% for $0.13 < d/A_{b,PE,eq} < 0.21 \text{ m}^{-1}$ and for $3.1 \cdot 10^{-3} < d/A_{b,PE,eq} < 4.9 \cdot 10^{-3} \text{ m}^{-1}$ respectively,
 541 as illustrated in Figure 11b.



542 **Figure 11.** CA based fragility curves for near collapse and life safety preventions with: a) HF_{aveq} as IM; b) $d/A_{b,PE,eq}$ as
 543 IM

544 It is interesting to note that in general, the fragility curves show lower probabilities of exceedance for
 545 a given value of IM when the probabilistic model for the steel strength at elevated temperature is
 546 considered (CS1-CS3 in Figure 10 and Figure 11). However, this may not be true for low probabilities
 547 of exceedance owing to the higher dispersions found in CS1 to CS3. This is a typical effect when
 548 considering parameter uncertainties, as the introduction of further uncertainties inflates the tails of
 549 the probability distributions, causing their cumulative distributions, i.e., the fragility functions, to
 550 span over larger IM ranges. Nevertheless, the medians of the probability distributions, i.e., the values
 551 of IM for which a probability of exceedance of 50% is reached, are always less demanding for CS1-
 552 CS3. Therefore, it can be concluded that in general less severe fragility curves are obtained when the
 553 probabilistic model for the steel strength is considered. This was expected because the retention
 554 factors at elevated temperature included in Eurocode are for design purposes and thus, inherently
 555 conservative. Indeed, in the probabilistic model the retention factor k_y of the steel yield strength f_y
 556 in CS1 - CS3 is higher than the nominal one $k_{y,EN1993-1-2}$ used in CS0 (see Figure 3a).

557 In addition, the employment of probabilistic fire diameter distributions rather than a uniform one may
558 have a significant influence on the fragility curves (CS1 vs CS2 and CS3), whilst very similar curves
559 are always found for two normal diameter distributions with different mean and standard deviation
560 because of the different type of leakage, i.e. CS2 vs CS3. Hence, the fragility curves seem more
561 sensitive to the fact that a discrete diameter distribution is employed, rather than to the variation of
562 the mean and standard deviation of the diameter of continuous density probability distributions. It
563 should be noted that the difference in the mean and standard deviations of the normal distributions
564 between leakage from a hole and from a pipe is in the order of about 12%. Moreover, it cannot be
565 concluded that discrete diameter distributions always provide more severe fragility functions. Indeed,
566 as shown in Figure 11, CS2 and CS3 fragility curves may be more or less severe than the ones from
567 CS1 depending on the limit state and on the IM. Nevertheless, the definition of fire demand models
568 based on probabilistic distributions is desirable and should be preferred since they provide more
569 realistic fire scenarios based on leakage from a hole in the tank (CS2) or from a pipe (CS3).

570 **4. Conclusions**

571 The paper presented the development of probabilistic fire demand models for a prototype steel pipe-
572 rack exposed to localised fires by adding uncertainties related to the structural capacity, i.e. yield
573 strength, and to the fire diameter that is caused by a hole in a tank or by a hole in a pipe. PFDMs were
574 defined for each case study by means of the Cloud analysis (CA) and, when suitable, also through the
575 Multiple stripe analysis (MSA). It is shown that the CA is a viable method to derive PFDMs and fire
576 fragility curves, whilst in order to benefit from the application of MSA, suitable IMs should be
577 identified before performing the analyses so as to obtain stripes with at least 10 instances by scaling
578 the severity of the fire based on such IMs. As expected, by allowing for the uncertainty of the steel
579 yield strength, lower values of ISDR with respect to the reference case study CS0 were observed
580 because the retention factors, and in turn the yield strength values at elevated temperature were, on
581 average, larger than the ones prescribed in EN 1993-1-2. Indeed, the steel structural members

582 plasticized later with the probabilistic material model (CS1, CS2 and CS3), allowing for both a delay
583 in load redistribution and smaller displacements, therefore resulting in less severe fragility curves.
584 The fire fragility curves were derived for different EDP-IM candidates. In this respect, the most
585 suitable IMs for steel pipe-racks, with similar characteristics with the prototype one, exposed to
586 localised fires were identified as the ones that maximise the efficiency (lowest dispersion of the EDP
587 given the IM) and the relative sufficiency (highest amount of information on the structural response).
588 Three suitable IMs were identified: i) the fire position-diameter ratio L/D , which is easy to use for
589 practitioners, but has lower efficiency and relative sufficiency indicators among the three proposed
590 IMs; ii) the maximum average heat flux impinging the structure HF_{avg} and iii) the scaled distance
591 $d/A_{b,PE,eq}$, which consists of a simple function of the fire parameters q , d and D , derived in similar
592 fashion for explosion hazard as the structure-explosion distance over a fractional power of an
593 equivalent TNT mass. The HF_{avg} and the $d/A_{b,PE,eq}$ are more efficient and more relatively sufficient
594 IMs, but the maximum average heat flux impinging the structure HF_{avg} is not as straightforward to
595 calculate as the scaled distance $d/A_{b,PE,eq}$, that showed comparable efficiency and sufficiency with
596 HF_{avg} and accounts for the effects of the distance of the fire from the structure and the extension of
597 the fire. MSA based fragility curves with L/D as IM were developed for the CS0 and CS1, but only
598 7 analyses were available for some stripes and thus, the CA fragility functions are deemed more
599 reliable. Furthermore, probabilistic diameter distributions in CS2 and CS3 had influence on the
600 fragility curves by lowering the probability of exceedance of the limit states for same values of IM
601 and should be considered since they provide more realistic fire scenarios. In general, the definition of
602 fire demand models based on probabilistic distributions for demand and capacity is desirable and
603 should be preferred since they provide more realistic fire scenarios. Future perspectives will focus on
604 considering multiple burning pool fires and the presence of the wind.

605 **Acknowledgements**

606 This research has been funded by the European XP-Resilience project through the grant agreement
607 number 721816. The support received from the Italian Ministry of Education, University and

608 Research (MIUR) in the frame of the ‘Departments of Excellence’ (grant L 232/2016) is gratefully
609 acknowledged. The first author was partially supported by the UK Research and Innovation (UKRI)
610 Institution in the framework of the project RESTORE (grant EP/X032469/1).

611 **Funding**

612 Ministero dell’Istruzione, dell’Universita` e della Ricerca; Grant: L 232/2016. Horizon 2020
613 Framework Programme; Award number: 721816; Recipient: Jerome Randaxhe.

614 **References**

- 615 1. European Comitee for Standardisation (2002). Eurocode 1 Actions on structures – Part 1–2: General
616 actions – actions on structures exposed to fire.
- 617 2. Franssen JM, Gernay T. Modeling structures in fire with SAFIR®: theoretical background and
618 capabilities. *J Struct Fire Eng* 2017;8(3):300–23.
- 619 3. Bailey, C. G. 1998. “Development of computer software to simulate the structure behaviour of steel-
620 framed buildings in fire.” *Comput. Struct.* 67 (6): 421–438. [https://doi.org/10.1016/S0045-](https://doi.org/10.1016/S0045-7949(98)00096-0)
621 [7949\(98\)00096-0](https://doi.org/10.1016/S0045-7949(98)00096-0).
- 622 4. ABAQUS. 2014a. ABAQUS version 6.14, User’s manual. Vélizy-Villacoublay, France: Dassault
623 Systèmes.
- 624 5. ANSYS Inc. 2016. ANSYS versrefboion 17.0, User’s manual. Canonsburg, PA: ANSYS.
- 625 6. DIANA FEA BV. 2016. DIANA version 10.1, User’s manual. Delft, Netherlands: DIANA FEA BV.
- 626 7. Possidente L., Tondini N., Battini J.-M. (2019). Branch-switching procedure for post-buckling
627 analyses of thin-walled steel members in fire. *Thin-Walled Structures* 136, 90-98.
- 628 8. Possidente L., Tondini N., Battini J.-M. (2020). 3D Beam Element for the Analysis of Torsional
629 Problems of Steel-Structures in Fire. *J. Struct. Eng.*, 146:(7), 10.1061/(ASCE)ST.1943-
630 541X.0002665.
- 631 9. Rackauskaite, E., Kotsovinos, P., Rein, G. (2017). Structural response of a steel-frame building to
632 horizontal and vertical travelling fires in multiple floors. *Fire Saf. J.* 91, 542–552.
633 <http://dx.doi.org/10.1016/j.firesaf.2017.04.018>

- 634 10. Gernay, T., Khorasani, N.E. (2020). Recommendations for performance-based fire design of
635 composite steel buildings using computational analysis. *J. Constr. Steel Res.* 166.
636 <https://doi.org/10.1016/j.jcsr.2019.105906>
- 637 11. Possidente L., Tondini N., Battini J.-M. (2020). Torsional and flexural-torsional buckling of
638 compressed steel members in fire. *Journal of Constructional Steel Research*: 171
- 639 12. Bergmeister, K., Brunello, P., Pachera, M., Pesavento, F., Schrefler, B.A. (2020). Simulation of fire
640 and structural response in the Brenner Base Tunnel by means of a combined approach: A case study.
641 *Eng. Struct.* 211. <https://doi.org/10.1016/j.engstruct.2020.110319>
- 642 13. Possidente L., Weiss A., de Silva D., Pustorino S., Nigro E., Tondini N. (2021) Fire safety engineering
643 principles applied to a multi-storey steel building, *Proceedings of the Institution of Civil Engineers -*
644 *Structures and Buildings*, 174(9), pp. 725-738, <https://doi.org/10.1680/jstbu.20.00110>
- 645 14. Bilotta A., de Silva D., Nigro E. (2016) General approach for the assessment of the fire vulnerability
646 of existing steel and composite steel concrete structures, *Journal of Building Engineering*: 8, 198-207.
- 647 15. Mackie KR, Stojadinovic B. (2005) Comparison of incremental dynamic, cloud, and stripe methods
648 for computing probabilistic seismic demand models. In: *Structures congress*.
649 [https://doi.org/10.1061/40753\(171\)184](https://doi.org/10.1061/40753(171)184)
- 650 16. Shome N, Cornell CA, Bazzurro P, Carballo JE. (1998) Earthquakes, records, and nonlinear responses.
651 *Earthq Spectra*;14:469–500.
- 652 17. Cornell CA, Jalayer F, Hamburger RO, Foutch DA (2002). Probabilistic basis for 2000 SAC federal
653 emergency management agency steel moment frame guidelines. *J Struct Eng*: 526–33.
- 654 18. Baker JW. (2015) Efficient analytical fragility function fitting using dynamic structural analysis.
655 *Earthq Spectra*;31:579–99.
- 656 19. Luco N, Cornell CA. (2007) Structure-specific scalar intensity measures for near-source and ordinary
657 earthquake ground motions. *Earthq Spectra*;23(2):357–92.
- 658 20. Ebrahimian H, Jalayer F, Lucchini A, Mollaioli F, Manfredi G. (2015) Preliminary ranking of
659 alternative scalar and vector intensity measures of ground shaking. *Bull Earthq Eng*:2805–40.

- 660 21. Nigro, E., Bilotta, A., Asprone, D., Jalaver, F., Prota, A., Manfredi, G., (2014). Probabilistic approach
661 for failure assessment of steel structures in fire by means of plastic limit analysis. *Fire Saf. J.* 68, 16–
662 29.
- 663 22. Gernay T, Khorasani NE, Garlock M.(2016) Fire fragility curves for steel buildings in a community
664 context: a methodology. *Eng Struct*;113:259–76.
- 665 23. Gernay T, Khorasani NE, Garlock M. (2019) Fire fragility functions for steel frame buildings:
666 sensitivity analysis and reliability framework. *Fire Technol*;55(4): 1175–210.
- 667 24. Lange D, Devaney S, Usmani A. (2014) An application of the PEER performance based earthquake
668 engineering framework to structures in fire. *Eng Struct*;66: 100–15.
- 669 25. Shrivastava M, Abu AK, Dhakal RP, Moss PJ. (2019) Severity measures and stripe analysis for
670 probabilistic structural fire engineering. *Fire Technol*;55(4):1147–73.
- 671 26. Cornell CA, Krawinkler H. (2003) Progress and challenges in seismic performance assessment. *Peer*
672 *Cent News*;3(2):1–3
- 673 27. Campedel M. (2008) Analysis of major industrial accidents triggered by natural events reported in the
674 principal available chemical accident databases. University of Bologna, European Commission Joint
675 Research Centre Institute for the Protection and Security of the Citizen.
- 676 28. Paolacci F. (2010) Structural safety of industrial steel tanks; pressure vessels and piping – basic
677 seismic structural design of a typical piping system. University of RomaTre.
- 678 29. Bursi O, Paolacci F, Reza MS, Alessandri S, Tondini N. (2010) Seismic assessment of petrochemical
679 piping systems using a performance-based approach. *J Press Vessel Technol*.
- 680 30. Paolacci F, Bursi O, Reza MdS, Kumar A, Gresnigt AM. (2013) Main issues on the seismic design of
681 industrial piping systems and components. In: *ASME 2013 pressure vessels & piping division*
682 *conference*; p. 1–10.
- 683 31. Bursi O, Paolacci F, Reza MS. (2015) Performance-based analysis of coupled support structures and
684 piping systems. In: *ASME 2015 pressure vessels & piping division conference*; no. July.
- 685 32. Bernier C, Padgett JE. (2019) Fragility and risk assessment of aboveground storage tanks subjected to
686 concurrent surge, wave, and wind loads. *Reliab Eng Syst Saf* no.February.

- 687 33. Uehara V. (1991) Fire safety assessments in petrochemical plants. In: Fire safety science – third
688 international symposium; p. 83–96.
- 689 34. Chang JI, Lin C. (2005) A study of storage tank accidents. *J Loss Prev Process Ind*;19:51–9.
- 690 35. Zheng B, Chen G. (2011) Storage tank fire accidents. *Process Saf Prog*;30(3).
- 691 36. Shu C, Chong C. (2009) Applications of 3D QRA technique to the fire/explosion simulation and
692 hazard mitigation within a naphtha-cracking plant. *J Loss Prev Process Ind*;22(4):506–15.
- 693 37. Committee for the prevention of disasters by hazardous materials (2005) Methods for the calculation
694 of physical effects due to releases of hazardous materials – Yellow Book. Gevaarlijke Stoffen, The
695 Hague.
- 696 38. Vílchez JA, Espejo V, Casal J. (2011) Generic event trees and probabilities for the release of different
697 types of hazardous materials. *J Loss Prev Process Ind*;24(3):281–7.
- 698 39. Moosemiller M. (2011) Development of algorithms for predicting ignition probabilities and explosion
699 frequencies. *J Loss Prev Process Ind*;24(3):259–65.
- 700 40. Gottuk DT, White DA. (2016) Liquid fuel fires. *SFPE Handb Fire Prot Eng*;12:2552–90.
- 701 41. Elhami Khorasani N, Gardoni P, Garlock M. (2015) Probabilistic fire analysis: material models and
702 evaluation of steel structural members. *J Struct Eng ASCE* 141(12)
- 703 42. Qureshi R, Ni S, Elhami Khorasani N, Van Coile R; Hopkin, Gernay T (2020) Probabilistic Models
704 for Temperature-Dependent Strength of Steel and Concrete. *J Struct Eng ASCE* 146(6)
- 705 43. Randaxhe J, Popa N, Tondini N (2021) Probabilistic fire demand model for steel pipe-racks exposed
706 to localised fires. *Engineering Structures* 226
- 707 44. Thomas PH. (1963) The size of flames form natural fires. In: Symposium international on combustion,
708 vol. 9. p. 844–59.
- 709 45. Mudan KS. (1984) Thermal radiation hazards from hydrocarbon pool fires. *Prog Energy Combust*
710 *Sci*;10:59–80.
- 711 46. Heskestad G. (1984) Engineering relations for fire plumes. *Fire Saf J*;7(2):25–32.
- 712 47. Rew PJ, Hulbert WG. (1996) Development of pool fire thermal radiation model. In: HSE Contract
713 Research Report.

- 714 48. Babrauskas V. (1983) Estimating large pool fire burning rates. *Fire Technol*:251–61.
- 715 49. Shokri M, Beyler CL. (1989) Radiation from large pool fires. *SFPE J Fire Protect Eng*; 4(1):141–50.
- 716 50. Society of Fire Protection Engineers (2016) *SFPE handbook of fire protection engineering*. 6th ed.
- 717 US: Springer.
- 718 51. Kamikawa D, Hasemi Y, Wakamatsu T, Kagiya K. (2003) Experimental flame heat transfer
- 719 correlations for a steel column adjacent to and surrounded by a pool fire. *Fire Saf Sci - Seventh Int*
- 720 *Symp*:989–1000. <https://doi.org/10.3801/IAFSS.FSS.7-989>.
- 721 52. Hanus F, Vassart O, Tondini N, Nadjai A, Franssen J. (2016) Temperature assessment of a vertical
- 722 steel member subjected to localised fire: experimental tests. In: *Proceedings of the 9th conference on*
- 723 *structures in fire*.
- 724 53. Tondini N, Franssen J-M. (2017) Analysis of experimental hydrocarbon localised fires with and
- 725 without engulfed steel members. *Fire Saf J*;92(May):9–22.
- 726 54. Francis P, Baddo N, Hanus F, Thauvoye C. (2018) *Design of columns subject to localised fires*. The
- 727 *Steel Construction Institute (SCI)*.
- 728 55. Tondini N, Thauvoye C, Hanus F, Vassart O. (2019) Development of an analytical model to predict
- 729 the radiative heat flux to a vertical element due to a localised fire. *Fire Saf J*;105(March):227–43.
- 730 56. Yamaguchi T., Wakasa K. (1986). Oil pool fire experiment. In: *Fire Safety Science – First*
- 731 *international symposium*. pp. 911–18.
- 732 57. European Comitee for Standardisation (2005). *Eurocode 3 Design of steel structures - Part 1-2:*
- 733 *General rules - Structural fire design*.
- 734 58. Zabetakis MG, Burgess DS. (1960). *Research on the hazards associated with the production and*
- 735 *handling of liquid hydrogen*, Ohio, USA.
- 736 59. Drysdale D. (2011) *An introduction to fire dynamics*. 3rd ed. John Wiley & Sons.
- 737 60. Van Coile R., Elhami Khorasani N., Lange D., Hopkin D. (2021) Uncertainty in Structural Fire
- 738 *Engineering*, *International Handbook of Structural Fire Engineering*, pp 323–411
- 739 61. Singh. K., Gardoni P., Stochino F. (2020). Probabilistic models for blast parameters and fragility
- 740 estimates of steel columns subject to blast loads, *Engineering Structures*;222

- 741 62. Song X. (2020). Parameterized fragility analysis of steel frame structure subjected to blast loads using
742 Bayesian logistic regression method, *Structural Safety*; 87
- 743 63. Zhang C., Gholipour G., Mousavi A. A. (2019). Nonlinear dynamic behavior of simply-supported RC
744 beams subjected to combined impact-blast loading. *Engineering Structures*;181:124-142
- 745 64. FEMA and ASCE, (2000) FEMA 356 – Prestandard and commentary for the seismic rehabilitation of
746 buildings, no. November. Federal Emergency Management Agency.
- 747 65. Phan H, Paolacci F, Corritore D, Tondini N, Bursi O, (2019) A Kriging-Based Surrogate Model for
748 Seismic Fragility Analysis of Unanchored Storage Tanks, ASME 2019 Pressure Vessels & Piping
749 Conference